

Decoder-side Cross Resolution Synthesis for Video Compression Enhancement

Ming Lu, Tong Chen, Zhenyu Dai, Dong Wang, Dandan Ding, and Zhan Ma, *Senior Member, IEEE*

Abstract—This paper proposes a decoder-side Cross Resolution Synthesis (CRS) module to pursue better compression efficiency beyond the latest Versatile Video Coding (VVC), where we encode intra frames at original high resolution (HR), compress inter frames at a lower resolution (LR), and then super-resolve decoded LR inter frames with the help from preceding HR intra and neighboring LR inter frames.

For a LR inter frame, a motion alignment and aggregation network (MAN) is devised to produce temporally aggregated motion representation to best guarantee the temporal smoothness; Another texture compensation network (TCN) is utilized to generate texture representation from decoded HR intra frame for better augmenting spatial details; Finally, a similarity-driven fusion engine synthesizes motion and texture representations to upscale LR inter frames for the removal of compression and resolution re-sampling noises.

We enhance the VVC using proposed CRS, showing averaged 8.76% and 11.93% Bjøntegaard Delta Rate (BD-Rate) gains against the latest VVC anchor in Random Access (RA) and Low-delay P (LDP) settings respectively. In addition, experimental comparisons to the state-of-the-art super-resolution (SR) based VVC enhancement methods, and ablation studies are conducted to further report superior efficiency and generalization of the proposed algorithm. All materials will be made to public at <https://njuvision.github.io/CRS> for reproducible research.

Index Terms—Video Coding, Cross Resolution Synthesis, Super Resolution, Deep Learning.

I. INTRODUCTION

Over decades, academic researchers and industrial practitioners have been continuously pursuing higher video coding efficiency for better transmission and storage since compressed video services have been overwhelmingly prevailing the entire Internet. It has led to a serial well-engineered video coding standards, including the H.264/Advanced Video Coding (AVC) [1], H.265/High-Efficiency Video Coding (HEVC) [2], and the Versatile Video Coding (VVC). On the other hand, built upon the advancement of deep neural networks (DNNs), a number of DNN-based end-to-end trainable video coding methods have emerged [3]–[6] recently with encouraging improvement on compression efficiency. All of these attempt to develop a set of new tools in coding loop or even new coding standard frameworks to exploit redundancy across intra and inter frames for compact representation, mainly assuming the fixed spatiotemporal resolution to process every frame uniformly.

Alternatively, enhancing decoded video frames in post-processing module is another means to improve overall quality

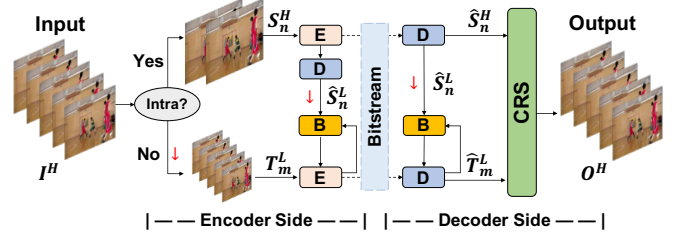


Fig. 1. CRS-based Video Compression Enhancement (VCE). ↓ (in red) is for bicubic down-sampling; E, D, and B represent video encoder, decoder, and decoded picture buffer (DPB) respectively.

under the same bit rate budget. Popular examples include quality enhancement for compression artifacts reduction, super resolution (SR) for original resolution restoration, etc [7]–[13]. Such decoder-side video compression enhancement (VCE) approaches can be quickly enabled for existing video codecs massively deployed in products, attracting intensive attention for network constrained video applications. For decoder-side SR, it often uniformly downsamples all frames of the input video to a lower resolution for encoding, and then upsamples decoded frame to its original resolution thereafter. Despite noticeable coding gains have been reported for various learnt SR based VCE [13]–[16], the performance still suffers for videos with irregular motion and complex texture that are difficult to restore, particularly at relatively high bit rates [17]–[19]. This work is another example belonging to such decoder-side SR category, targeting for better compression efficiency across a variety of bitrates and video sources.

A. General Structure

Generally, we propose to non-uniformly sample the input video for compression. For a given group of pictures (GoP), the first frame is intra-coded while the rest of them in this GoP are inter-coded. We downscale inter frames to a lower spatial resolution, while keeping intra frames at the same frame size as the input video, as shown in Fig. 1. Ideally, we wish to use original high-resolution (HR)¹ intra frame to preserve spatial texture details, and have downsampled low-resolution (LR) inter frames to capture the temporal motion smoothness.

We encode HR intra frame and LR inter frames using the latest VVC model. Other standards such as the HEVC can be applied as well. HR intra frames is coded, reconstructed,

¹The term “high-resolution” is a relative phrase to the downsampled “low-resolution”. The spatial resolution of intra frame is actually the same as the input video.

and downsampled to the same size as the LR inter frames before being put into the decoded picture buffer (DPB) to perform motion estimation and residual coding as in Fig. 1. Compressed sub-streams of respective HR intra and LR inter frames are then multiplexed and delivered to the receiver for decoding.

Prior to being displayed to end user, decoded HR intra and LR inter frames² are synthesized to produce high-fidelity video at its input resolution. Such *cross-resolution synthesis* aims to alleviate compression and re-sampling noises so as to preserve both spatial details and temporal smoothness through spatiotemporal correlation exploration.

B. Key Module

The proposed CRS utilizes the spatial details from preceding HR intra frame and temporal smoothness from neighboring LR inter frames to super-resolve current LR inter frame.

Thus, we first devise a motion alignment and aggregation network (MAN) to generate temporal motion representation of current LR inter frame by aggregating the information across a set of consecutive neighboring frames. This MAN is comprised of a deformable convolution network [20]-based multi-frame motion feature alignment and a separable temporal-spatial attention-based motion feature aggregation;

In the meantime, we feed decoded LR inter frames, decoded HR intra frame as well as its re-sampled version into a texture compensation network (TCN) to learn multiscale affinity map for the representation of cross-resolution correlation and generate multiscale texture representation for better augmenting spatial details. This TCN patch-wisely matches similar features between HR intra and LR inter frame for efficient texture transfer [21], [22].

Finally, a similarity-driven fusion is used to intelligently synthesize current LR inter frame using aggregated motion representation from the MAN, and both multiscale affinity map and multiscale texture representation from TCN model.

Because of the information propagation across all frames within current GoP, a reference frame (a.k.a., HR intra frame) with better reconstruction quality would have great impact on the reconstruction quality of succeeding LR inter frames. Thus, we have also carefully examined the quantization parameter (QP) allocation to properly assign QPs across intra and inter frames for better compression performance.

C. Performance

To exemplify the performance of proposed CRS-based VCE, this work uses bicubic filter in default for down-sampling and applies VVC compliant RA and LDP encoders for compression. All other parameters are closely following the common test conditions (CTC) suggested by the standardization committee [23]. The proposed CRS-based VVC enhancement, or “CRS (bicubic)” for short in Tables II, III,

²Since proposed CRS and other SR methods in this study basically process “decoded frames” or “decoded intra/inter frames” for enhancement. For simplicity, we sometimes call them intra/inter frame directly by omitting the term “decoded”.

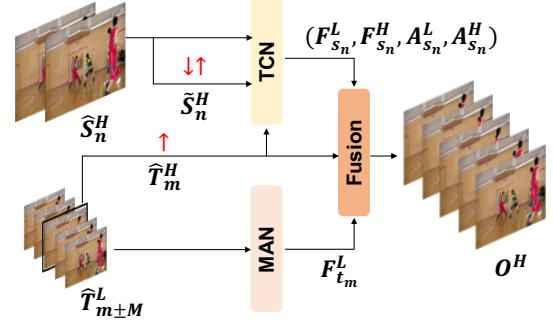


Fig. 2. **The CRS Model** is comprised of three modular components: a motion alignment and aggregation network (MAN) for generating aggregated motion representation, a texture compensation network (TCN) is for fine-grained multiscale texture representation and corresponding multiscale affinity map, and a similarity-driven fusion engine to super-resolve input LR inter frame by intelligently combining outputs from the MAN and TCN. \downarrow and \uparrow (in red) are bicubic filter for downsampling and upsampling.

and V, achieves remarkable compression efficiency improvement, e.g., approximately 8.76% and 11.93% BD-Rate [24]³ savings against the anchor VVC reference model VTM 10.0 (<https://jvet.hhi.fraunhofer.de/>) in RA and LDP configurations respectively.

Additional comparisons to traditional SR-based VCE using interpolation filter (e.g., bicubic and lanczos) and state-of-the-art SR methods (e.g., RCAN [15] and EDVR [16]) for uniform upsampling have further revealed the superior efficiency of our method. As also reported in JVET EE summary report [23], our method presents clear lead against two alternative SR methods, a.k.a., JVET-V0073 [11] and JVET-V0096 [12].

Ablation studies then report the robustness and generalization of proposed solution by carefully examining a variety of different settings. A companion material is also provided when setting the HEVC reference model as the compression engine, reporting even greater coding gains (e.g., >20% BD-Rate gains for LDP scenario). Such noticeable gains are potentially attractive to those HEVC compliant video services.

D. Contribution

1) We non-uniformly sample intra and inter frames for compression, in which we keep intra frame at the same resolution as the input video to retain spatial details, and downscale inter frames to a lower resolution to capture motion smoothness; and then devise the Cross Resolution Synthesis to fuse decoded HR intra and LR inter frames for final high-fidelity reconstruction. This probably is the *first work* utilizing cross resolution synthesis for accurately aggregating necessary information from non-uniformly sampled intra and inter frames.

2) The CRS includes a MAN and a TCN to respectively retain temporal smoothness and spatial details for reconstruction synthesis through similarity-driven fusion. And, a QP

³Following the CTC rules mandated by the standardization committee, we mainly report the BD-Rate using widely-adopted PSNR based distortion measurement. Other distortion measures, such as the multiscale structural similarity, and VMAF [25], present the similar performance lead for our proposed CRS.

TABLE I
ABBREVIATIONS FREQUENTLY USED IN THIS WORK

Abbr.	Description
CRS	Cross Resolution Synthesis
SR	Super Resolution
VCE	Video Compression Enhancement
DNN	Deep Neural Networks
MAN	Motion Alignment and Aggregation Network
TCN	Texture Compensation Network
DCN	Deformable Convolutional Network
GoP	Group of Pictures
QP	Quantization Parameter
DPB	Decoded Picture Buffer
R-D	Rate-Distortion
BD-Rate	Bjontegaard Delta Rate
PSNR	Peak Signal-to-Noise Ratio
RA	Random Access
LDP	Low-Delay P
VVC	Versatile Video Coding
HEVC	High-Efficiency Video Coding
JVET	Joint Video Exploration Team
EE	Exploration Experiment

allocation strategy is also applied to further improve the overall R-D performance.

3) Our CRS-based VVC enhancement shows remarkable coding gains over the latest VVC reference model, and also significantly outperforms other SR-based methods with clear performance lead. Note that our CRS fundamentally complies with all popular video codec, promising the encouraging application prospect.

The paper is organized as follows. In Section II, relevant studies are briefly reviewed. Section III formulates the problem by analyzing the noise incurred in compression and re-sampling processes. The proposed cross-resolution synthesis is described in Section IV, followed by experimental studies in Section VI. Finally, the paper is concluded in Section VII. For convenience, we put all abbreviations and notations in Table I.

II. RELATED WORK

This section reviews relevant algorithms for decoder-side video compression enhancement.

A. Resolution Adaptation based Video Coding

More than a decade ago, a region-based video coding method was brought up in [26] where input high-resolution image sequences were down-sampled and compressed; Correspondingly, compressed bitstream was decoded and then super-resolved to the same resolution as its input. Note that additional region segmentation metadata used for classifying the motion and texture blocks, was encapsulated as the side information for more efficient decoder-side super resolution. Then, key frame classification was introduced in [27] by which down-sampling was only enabled for non-key frames prior to being encoded. The reconstruction was fulfilled by block-matching based motion compensation and super resolution. Similar idea was further examined in [17] where intra-coded frames were key frames, and inter-coded frames were non-key frames. And, LR inter-frames were restored using an example-based SR method. This idea was similar to our proposed CRS to some extent but they did not efficiently leverage

the texture information of the reference (or key) frames for reconstruction. More recently, deep learning-based single image SR was suggested by [19], [28] to upscale all decoded LR frames for quality enhancement. These methods did not differentiate frame types and fully relied on powerful DNNs to recover down-sampling-induced high-frequency information loss. For those SR-based video compression enhancement, better coding performance was only captured for low bit rates within a narrow range since they could hardly restore the high-frequency details which are critical at relatively high bit rates.

B. Learnt Super-Resolution

The coding gains of SR-based VCE is heavily dependent on the efficiency of SR algorithm. In past few years, deep learning-based SR methods have shown great improvement to conventional handcrafted algorithms. For example, a single image SR network utilizing several modified residual blocks [29] was developed in [30]. Later, the channel attention mechanism was proposed in [15] to further improve the performance of single image SR. Such single image SR methods were then extended to multi-frame SR by aggregating temporal information across neighbor frames. Shi *et al.* [31] first proposed a DNN-based multi-frame SR method, for which the optical flow was used to align adjacent frames for subsequent fusion. The performance of multi-frame SR was improved noticeably as reported in [16] by applying a pyramid deformable convolution network [20] and an attention based network to efficiently align spatiotemporal features across frames. These multi-frame SR methods had presented clear performance lead to single image SR methods by jointly exploiting the spatial and temporal correlations.

III. PROBLEM FORMULATION

As shown in Fig. 1, for every GoP, our CRS-based VCE approach directly encodes the HR intra frame and LR inter frames. The decoded HR intra frame is then down-sampled and put into the encoding and decoding buffer as the reference for the coding of succeeding LR inter frames; Subsequently, both decoded HR intra and LR inter frames are used to restore the output video at the same resolution as the input through proposed CRS.

We use a two-frame GoP where the first frame is intra frame and the second one is inter frame to exemplify the problem. As aforementioned, we wish to use HR intra frame \mathbf{S}^H to preserve spatial texture details and use LR inter frames \mathbf{T}^L to capture temporal motion smoothness, for final fusion (see Fig. 2).

More specifically, the HR intra frame \mathbf{S}_n^{H4} is first encoded with the introduction of compression noise $\varepsilon_{s_n}^Q$,

$$\hat{\mathbf{S}}_n^H = \mathbf{S}_n^H + \varepsilon_{s_n}^Q. \quad (1)$$

Here $\hat{\mathbf{S}}_n^H$ denotes the reconstructed HR intra frame, which is then downsampled to the same resolution as the LR inter

⁴We use the letters “S” and “T” for respective intra and inter frame; subscripts “n” and “m” to distinguish the frame order; and superscripts “H” and “L” for original high-resolution and downsampled low-resolution representation.

frames and buffered in the DPB for encoding upcoming LR inter frames, i.e.,

$$\hat{\mathbf{S}}_n^L = (\hat{\mathbf{S}}_n^H) \downarrow_d + \varepsilon_{s_n}^A, \quad (2)$$

where $(\cdot) \downarrow_d$ represents the down-sampling operation at a factor of d ($d = 2$ used in this paper for common practice which is also suggested in JVET EE [23]), $\varepsilon_{s_n}^A$ is the acquisition error induced by down-sampling.

Note that Equation (2) is applied to all input inter frames \mathbf{T}_m^H to produce their low-resolution counterparts, i.e.,

$$\mathbf{T}_m^L = (\mathbf{T}_m^H) \downarrow_d + \varepsilon_{t_m}^A. \quad (3)$$

Recalling that inter prediction exploits the temporal redundancy in video coding, it inherently will propagate the noise accumulated in reference to successive frames. Then the prediction of LR inter frames can be referred to as

$$\tilde{\mathbf{T}}_m^L = \mathcal{D}(\vec{v}_{t_m, s_n}) \cdot \hat{\mathbf{S}}_n^L + \varepsilon_{t_m, s_n}^R + \varepsilon_{t_m}^A. \quad (4)$$

Here $\hat{\mathbf{S}}_n^L$ is the reference frame of $\tilde{\mathbf{T}}_m^L$. $\mathcal{D}(\vec{v}_{t_m, s_n})$ is a displacement operation (e.g., warping) using a 2-D matrix \vec{v}_{t_m, s_n} as the pixel-level spatial offset between $\hat{\mathbf{S}}_n^L$ and \mathbf{T}_m^L . And, ε_{t_m, s_n}^R is the temporal registration error incurred by the inaccurate displacement. Then, motion vectors and residuals between the original inter frame \mathbf{T}_m^L and its prediction $\tilde{\mathbf{T}}_m^L$ are compressed, producing the reconstruction with accumulated noises:

$$\hat{\mathbf{T}}_m^L = \mathcal{D}(\vec{v}_{t_m, s_n}) \cdot \hat{\mathbf{S}}_n^L + \varepsilon_{t_m, s_n}^R + \varepsilon_{t_m}^Q + \varepsilon_{t_m}^A, \quad (5)$$

where both the acquisition error $\varepsilon_{s_n}^A$ and compression noise $\varepsilon_{s_n}^Q$ contained in $\hat{\mathbf{S}}_n^L$ are propagated to $\hat{\mathbf{T}}_m^L$ due to temporal referencing.

Although above we show only a simple example using a two-frame GoP, our framework can be extended to practical scenarios with arbitrary GoP size and coding configurations (e.g., RA or LDP). At decoder side, we wish to restore $\hat{\mathbf{T}}_m^L$ to its original resolution and alleviate the compound noises incurred by re-sampling, quantization, as well as the inter prediction.

Let $\mathbf{I}_{t_m}^H$ be labelled ground truth of inter frame \mathbf{T}_m^H , and $\mathbf{O}_{t_m}^H$ be the cross-resolution super-resolved result. Conceptually, we want to minimize their distance,

$$\min \|\mathbf{O}_{t_m}^H - \mathbf{I}_{t_m}^H\|, \text{ with } \mathbf{O}_{t_m}^H = \mathcal{S}\{\hat{\mathbf{T}}_m^L, \hat{\mathbf{S}}_n^H\}. \quad (6)$$

The distance is measured by the L1 loss, e.g., mean absolute error in this work. $\mathcal{S}\{\cdot\}$ is used for decoder-side CRS operation, in which we want to accurately characterize the spatial and temporal information for the restoration of current LR inter frame $\hat{\mathbf{T}}_m^L$. For practical implementation, Eq. (6) can be easily extended for supporting more LR inter frame in a GoP. More details of our proposal is given below.

IV. DECODER-SIDE CROSS-RESOLUTION SYNTHESIS

A. Overview

Ideally, we wish to restore high-frequency component loss induced by the compression and re-sampling in (5). In our approach, we attempt to leverage multiple temporal frame

neighbors to improve restoration quality and to guarantee the temporal motion smoothness of all super-resolved LR inter frames; Meanwhile, we also want to augment spatial details from the reconstructed HR intra frames to greatly alleviate such loss in LR inter frames.

Thus, the key problem behind is how to intelligently combine temporal motion features and spatial texture features to better super-resolve LR inter frames. In practice, we decompose the overall CRS optimization into three modular functions as in Fig. 2. Specifically, we leverage a MAN model to align and aggregate temporal motion features for a specific LR inter frame $\hat{\mathbf{T}}_m^L$ using its LR neighbors as well as itself, i.e.,

$$\mathbf{F}_{t_m}^L = \mathcal{M}_{\text{MAN}}\{\hat{\mathbf{T}}_{m-M}^L, \dots, \hat{\mathbf{T}}_m^L, \dots, \hat{\mathbf{T}}_{m+M}^L\}; \quad (7)$$

In the meantime, we propose another TCN model to characterize multiscale affinity map (texture correlation or similarity) $\vec{\mathbf{A}}_{s_n}$ and multiscale texture representation $\vec{\mathbf{F}}_{s_n}$ for compensation by inputting decoded HR intra frame $\hat{\mathbf{S}}_n^H$, resampled HR intra frame $\tilde{\mathbf{S}}_n^H$, and the upscaled version $\hat{\mathbf{T}}_m^H$ of current LR inter frame $\hat{\mathbf{T}}_m^L$, e.g.,

$$(\vec{\mathbf{F}}_{s_n}, \vec{\mathbf{A}}_{s_n}) = \mathcal{T}_{\text{TCN}}\{\hat{\mathbf{S}}_n^H, \tilde{\mathbf{S}}_n^H, \hat{\mathbf{T}}_m^H\}. \quad (8)$$

Finally, we leverage similarity-driven fusion to synthesize the input $\hat{\mathbf{T}}_m^L$ to its upscaled output $\mathbf{O}_{t_m}^H$ by properly weighing aforementioned spatiotemporal information, having

$$\mathbf{O}_{t_m}^H = \mathcal{S}\{\vec{\mathbf{F}}_{s_n}, \vec{\mathbf{A}}_{s_n}, \mathbf{F}_{t_m}^L, \hat{\mathbf{T}}_m^L\}. \quad (9)$$

Essentially, the cross-resolution synthesis shown in Eq. (9) can be easily extended to support any coding structures and any number of neighbors, such as the low-delay scenario using only preceding few neighbors.

B. Motion Alignment and Aggregation Network (MAN)

To guarantee the temporal smoothness and simultaneously to leverage temporal neighbors for better super-resolving LR inter frames, it is desired to accurately characterize motion dynamics across neighbor frames. The overall process generally includes feature alignment and aggregation as shown in Fig. 3.

1) *Alignment*: Recalling that multi-frame motion features are often used for temporal alignment [7], [16], we set $M = 1$, having a preceding and another succeeding frame besides current $\hat{\mathbf{T}}_m^L$ for a 3-frame temporal window buffer. Other temporal window buffer can be supported easily, such as only using preceding neighbor frames and/or even more number of neighbors.

First, a shared-weights feature extraction module consisting of 4 consecutive residual blocks [29] are devised to generate the deep feature representations of each frame in this temporal window buffer. The kernel size of convolution layers is fixed at 3×3 throughout this work. Since our task is aligning neighboring frames to current LR inter frame $\hat{\mathbf{T}}_m^L$, the remaining processes usually operate on frame (or feature) pairs where one of them is current frame (or deep features of current frame), and the other is one specific frame (or deep features of this specific frame) in temporal window buffer.

Deep features of frame pairs are concatenated and fed into a multiscale network (MSN) that consists of several residual

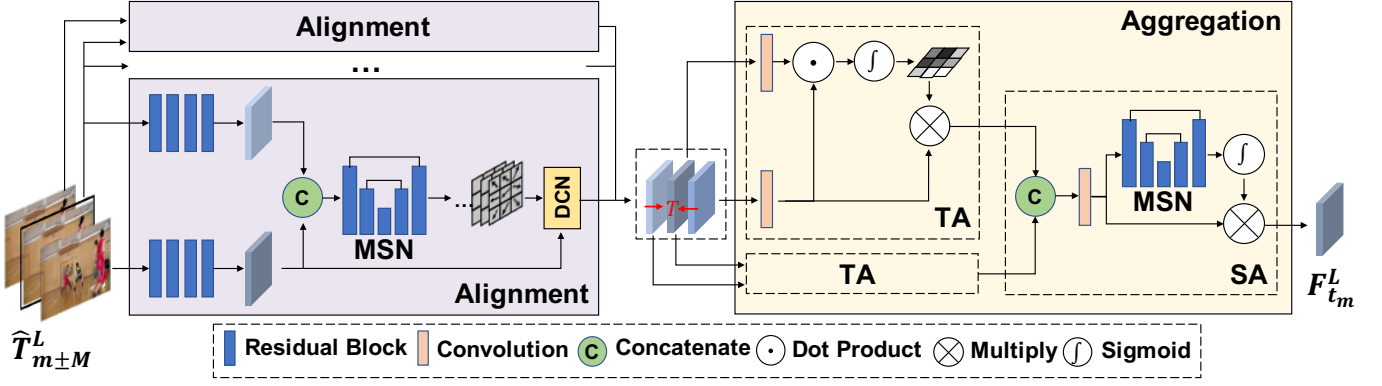


Fig. 3. **Motion Alignment and Aggregation Network (MAN)** for deriving aggregated motion representation. It consists of two stages: Alignment and Aggregation. At Alignment stage, 4 residual blocks are utilized to extract deep representative features of each LR inter frames; A multiscale network (MSN) is employed to generate the multiscale temporal offsets by traversing all pairs of current LR inter frame and each frame in temporal window buffer; Later, a deformable convolution network (DCN) is applied to generate aligned temporal features by inputting deep features of a neighbor frame and corresponding multiscale temporal offsets derived between this neighbor frame and current frame. Finally, separable temporal attention (TA) and spatial attention (SA) are consecutively applied to aggregate necessary and useful temporal motion features for temporally-smooth super-resolution. T is the total number of frames in temporal window buffer used for temporal alignment; $T = 2M + 1$ and it is 3 when having $M = 1$ in our implementation.

blocks for deriving the channel-wise temporal offsets between them. By deploying this multiscale model architecture, we can obtain more accurate temporal offsets for representing frame-wise motion displacement in feature domain [6], [32]. For the offsets derived using current frame and its neighbor, we call them cross-neighbor temporal offsets; and for the offsets computed using current frame and itself, we call them self-contained temporal offsets.

Subsequently, for a frame pair of current frame \hat{T}_m^L and another frame \hat{T}_x^L from the temporal window buffer, their aligned temporal features can be produced by inputting deep features of \hat{T}_x^L and corresponding learnt multiscale temporal offsets between \hat{T}_m^L and \hat{T}_x^L into the deformable convolution network (DCN) [20]. Though optical flows may fit for this task, they are very vulnerable to compression noises as exemplified in [32]. Thus we choose to use the DCN in this work. Then, following the same procedure, we iteratively align all frame pairs, producing T stacks of aligned temporal features, and each feature stack at a size of $\frac{H}{2} \times \frac{W}{2} \times C^6$. For a frame pair having current frame and its neighbor, their aligned temporal features are referred to as the neighbor-aligned temporal features; while for a frame pair having current frame and itself, it is self-aligned temporal features. T is the total number of frames in sliding temporal window buffer. As exemplified in Fig. 3, $T = 2M + 1 = 3$; Channel dimension C is 64, which is kept the same in this work; H and W are the height and width of the original input video.

2) *Aggregation*: We then apply attention-based mechanism to efficiently process multiple stacks of aligned temporal features by performing the separable temporal [16] attention (TA) and spatial [33] attention (SA)-based aggregation sequentially.

As illustrated in Fig. 3, such T stacks of aligned temporal features respectively describe alignment information of current frame and another frame in the sliding temporal window.

The similarity distance map of aligned temporal features is then calculated by applying the dot product on convoluted representations of the self-aligned temporal features and the other neighbor-aligned temporal features. This methodology has been widely used in attention network by transforming input data to another feature space (e.g., sometimes with fewer channels) to simplify the computation. By further applying the sigmoid activation function upon derived similarity distance map, we can get the temporal attention mask, which is then element-wisely multiplied with neighbor-aligned temporal features to have TA-optimized temporal features. Similar procedures are iteratively applied to other feature pairs including one stack of self-aligned temporal features and another stack of neighbor-aligned temporal features. Later, all TA-optimized temporal features are concatenated together and convoluted for subsequent spatial attention optimization.

In SA step, different from [33], we remove the max-pooling layer and employ the MSN (see SA box in Fig. 3) as well as sigmoid activation to generate the spatial attention masks to preserve the channel information. Thereafter, spatial attention mask is also multiplied element-wisely with the convoluted concatenation of all TA-optimized temporal features to produce final aggregated motion representation $F_{t_m}^L$ of current frame \hat{T}_m^L at a size of $\frac{H}{2} \times \frac{W}{2} \times C$. After all, this $F_{t_m}^L$ is expected to sufficiently carry temporal information learned by analyzing temporal dynamics across frames in the temporal window buffer, for better super-resolution.

Above deformable convolution based alignment and attention based aggregation can well capture the multi-frame spatiotemporal dynamics using pyramidal features. It could also overcome the challenging issues that could not be well handled by optical flow-based methods, such as noise, occlusion, and large motion displacement. [32]

C. Texture Compensation Network (TCN)

To restore the spatial texture details of decoded LR inter frames \hat{T}_m^L , one may use deformable convolutions or optical

⁵The subscript x indicates a specific frame in the temporal window buffer.

⁶This is because LR inter frame presents the downscaled size of $\frac{H}{2} \times \frac{W}{2}$ for luminance component.

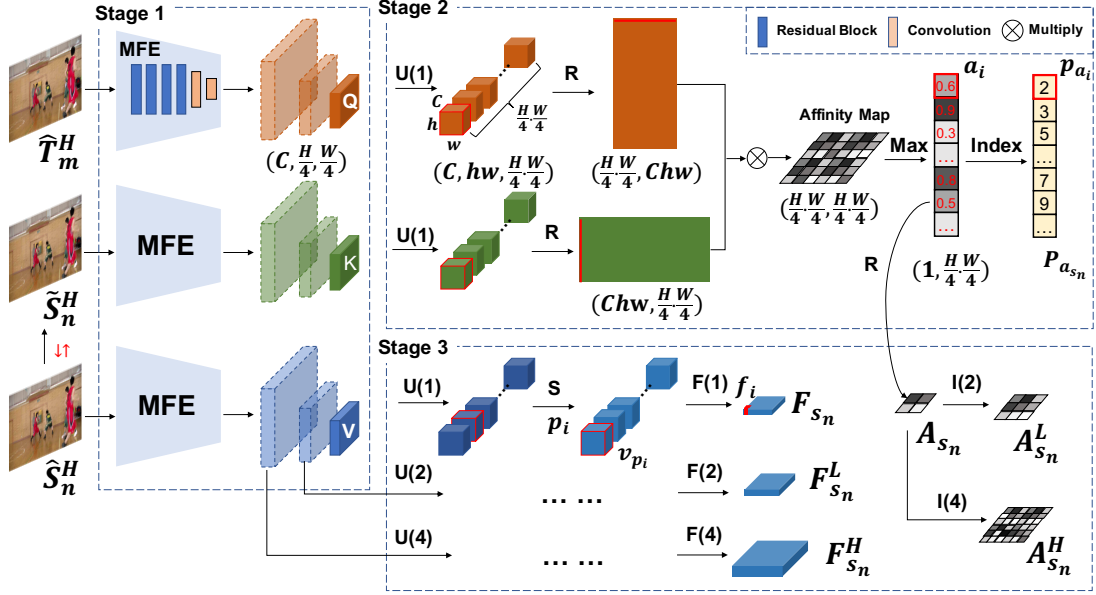


Fig. 4. **Texture Compensation Network (TCN)** for producing multiscale texture representation and multiscale affinity map. \uparrow (in red) denotes the re-sampling operation, $U(d)$ is for unfolding with stride d , R is for reshaping operation, S is index selection for patch re-organization, I is for interpolation, and $F(d)$ is for folding operation with stride d , which is the inverse operation of $U(d)$. The kernel sizes for $F(1)$, $F(2)$ and $F(4)$ are 3×3 , 6×6 and 12×12 respectively.

flow-based warping to align HR intra frame \hat{S}_n^H to current inter frame to help the super-resolved reconstruction. However, alignment efficiency degrades sharply as the frame distance between HR intra frame and associated LR inter frame increases, and so does the restoration quality of LR inter frame. Instead, motivated by recent texture transfer methods in [21], [22], [34], we introduce a texture compensation network (TCN) which resorts to patch-wise match to measure long-range similar features between the HR intra frame and current LR inter frame for fine-grained and robust texture transfer. The TCN basically consists of three processing stages to produce multiscale feature representation, feature domain correlation measurement, and multiscale spatial texture features.

1) *Stage 1 - Multiscale Feature Representation*: Ideally, we want to transfer sharp textures from the decoded HR intra frame \hat{S}_n^H to the current upscaled LR inter frame \hat{T}_m^H for better quality. To this end, we need to carefully examine their correlation and choose the most proper local patches for compensation. Note that \hat{T}_m^H is upscaled from its LR version \hat{T}_m^L . To alleviate the possible impact of re-sampling noises incurred in LR inter frames for correlation measurement, we propose to down-sample and then up-sample the decoded HR intra frame \hat{S}_n^H to \tilde{S}_n^H in the same way as inter frames.

Instead of directly performing pixel domain computation, we propose to perform feature domain exploration: capture the correlation of \tilde{S}_n^H and \hat{T}_m^H using multiscale feature representations that can better characterize fine-grained spatial texture dynamics. Towards this goal, we feed \tilde{S}_n^H , \hat{S}_n^H and \hat{T}_m^H separately into a shared-weights multi-scale feature extraction (MFE) module, which has four residual blocks and two convolutional layers with stride at 2. A set of multiscale features at different scale, a.k.a., Value (\mathbf{V}), Key (\mathbf{K}), and Query (\mathbf{Q}), are correspondingly generated for \tilde{S}_n^H , \hat{S}_n^H and

\hat{T}_m^H respectively, as illustrated in Fig. 4 (Stage 1).

2) *Stage 2 - Feature Domain Correlation Measurement*: We then define correlation measurement using the affinity calculation between \mathbf{Q} and \mathbf{K} . As then revealed by our extensive studies, utilizing respective \mathbf{Q} and \mathbf{K} features at the smallest scale (e.g., at a size of $\frac{H}{4} \times \frac{W}{4} \times C$), a.k.a, \mathbf{Q} and \mathbf{K} , can not only offers almost the same performance without noticeable degradation, but also reduces the computation significantly. Thus, we use the smallest scale features \mathbf{Q} and \mathbf{K} of \mathbf{Q} and \mathbf{K} for correlation derivation (e.g., affinity map, position map). Since such correlation metrics correspond to the smallest scale \mathbf{Q} and \mathbf{K} , they can be directly used to retrieve patches from the smallest scale component of \mathbf{V} , e.g., \mathbf{V} , for compensation.

Point-wise affinity measurement can be problematic between each element point in a feature map which can hardly describe the local information of target regions. Thus, as depicted in Fig. 4 (Stage 2), a $h \times w$ sliding window, e.g., $h = w = 3$, is used to transverse all feature element and unfold feature maps \mathbf{K} and \mathbf{Q} into local patches at a size of $[h, w, C]$ ⁷. Each patch \mathbf{k}_i for \mathbf{K} can be re-shaped to a vector at a size of $[1, Chw]$. Similarly, patch \mathbf{q}_j for \mathbf{Q} can be re-shaped to a vector at a size of $[1, Chw]$ as well. Here, $i, j \in [1, \frac{H}{4} \times \frac{W}{4}]$.

Then, we calculate the normalized cosine similarity to generate the affinity map in a non-local manner:

$$a_{i,j} = \langle \frac{\mathbf{k}_i}{\|\mathbf{k}_i\|}, \frac{\mathbf{q}_j}{\|\mathbf{q}_j\|} \rangle, \quad (10)$$

where $a_{i,j}$ denotes the relevance between patch \mathbf{k}_i and \mathbf{q}_j . As a result, for each \mathbf{q}_j in \mathbf{Q} , the most relevant patch \mathbf{k}_i in \mathbf{K} has the maximum correlation coefficient

$$a_i = \max_j a_{i,j}, \quad (11)$$

⁷Similar patch generation can be applied for \mathbf{V} as in Fig. 4 (Stage 3).

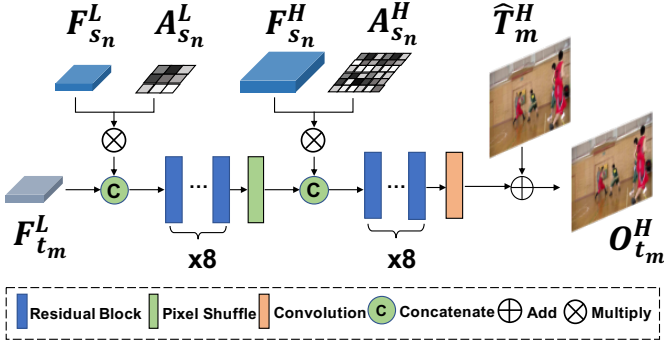


Fig. 5. **Similarity-driven Fusion** for final reconstruction synthesis. Scale-dependent fusion is applied to progressively combine affinity map, multiscale texture representation and aggregated motion representation for fine-grained spatiotemporal loss recovery.

and the position of the best k_i in \mathbf{K} is

$$p_{a_i} = \arg \max_j a_{i,j}. \quad (12)$$

Finally, we can construct the affinity map \mathbf{A}_{s_n} and its corresponding optimal patch position map $\mathbf{P}_{a_{s_n}}$ both at a size of $[1, \frac{H}{4} \times \frac{W}{4}]$ to represent the most relevant patches between \mathbf{K} and \mathbf{Q} by concatenating optimal a_i in (11) and p_{a_i} in (12) of each \mathbf{q}_j .

3) *Stage 3 - Multiscale Spatial Texture Features*: Following above discussions, we can utilize \mathbf{A}_{s_n} and $\mathbf{P}_{a_{s_n}}$ to retrieve the most proper patches from the smallest scale feature \mathbf{V} of HR intra frame for texture compensation. For example, we reorganize the patches of input \mathbf{V} using $\mathbf{P}_{a_{s_n}}$ to construct the smallest scale texture features \mathbf{F}_{s_n} at a size of $[\frac{H}{4}, \frac{W}{4}]$ (see Fig. 4 (Stage 3)).

Furthermore, we would like to use full-spectrum features of $\vec{\mathbf{V}}$ to best compensate the spatial frequency loss of LR frame. On the other hand, we have to keep the default size of optimal position map, otherwise, it may introduce aliasing or unexpected error due to incorrect retrieval position. Thus, for texture features of $\vec{\mathbf{V}}$ beyond the smallest scale, we apply the folding and unfolding operations with stride 2 and 4 respectively, to accurately align the positions with $\mathbf{P}_{a_{s_n}}$. At the unfolding step, we directly extract elements from feature maps; while in the opposite folding step, we plug the convolutions for better information embedding. Eventually, we will have $\mathbf{F}_{s_n}^L$ and $\mathbf{F}_{s_n}^H$ at sizes of $[\frac{H}{2}, \frac{W}{2}]$ and $[H, W]$ to form multiscale texture representation \mathbf{F}_{s_n} .

In the meantime, we bi-linearly interpolate \mathbf{A}_{s_n} at a factor of 2 and 4 both horizontally and vertically dimensions, respectively to have $\mathbf{A}_{s_n}^L$ and $\mathbf{A}_{s_n}^H$ which match the texture features of $\vec{\mathbf{V}}$ at another two scales to construct the multiscale affinity map $\hat{\mathbf{A}}_{s_n}$.

D. Similarity-driven Fusion

Till now, we have leveraged the MAN and TCN to generate spatial and temporal information respectively for final fusion. Specifically, we have $\vec{\mathbf{F}}_{s_n}$ to capture texture details from HR intra frame, $\hat{\mathbf{A}}_{s_n}$ to embed the similarity importance of relevant texture patches in HR intra frame, and $\mathbf{F}_{t_m}^L$ to

characterize the temporal smoothness across neighbor frames, which are then fused together with upsampled LR inter frame to its reconstruction in Eq. (9).

In practice, we synthesize the inputs at the same scale and progressively fuse them to the final output $\mathbf{O}_{t_m}^H$. Figure 5 illustrates the network structure in detail, where 8 residual blocks [29] are used to fuse the concatenation of aggregated motion representation, affinity map and texture representation at corresponding scale, i.e., (9) can be specifically re-written as

$$\mathbf{O}_{t_m}^H = \mathcal{S}\{\mathbf{F}_{s_n}^L, \mathbf{A}_{s_n}^L, \mathbf{F}_{s_n}^H, \mathbf{A}_{s_n}^H, \mathbf{F}_{t_m}^L, \hat{\mathbf{T}}_m^H\}, \quad (13)$$

where $\hat{\mathbf{T}}_m^H$ is upsampled from $\hat{\mathbf{T}}_m^L$ directly using the bicubic filter.

Note that Fig. 5 is exemplified for the case having one HR intra frame in LDP application. For RA configuration which has two HR intra frames for referencing, for which respective bidirectional multiscale texture representation and affinity maps will be generated and applied accordingly.

V. QP ALLOCATION

Because of the temporal referencing used in inter prediction, the quality of reference frame strongly impacts the encoding of the current frame. On the other hand, build upon the advancement of inter prediction tools [35], inter-coded frames occupy a small amount of compression bits compared with the intra-coded frame in a GoP. Note that LR inter frames consume even less bits because of the downsampled spatial resolution. According to our experimental studies, further lowering the QPs in HR intra frame does not actually improve the overall R-D efficiency because the distortion alleviation across HR intra and LR inter frames can not be well balanced by the bits increase of HR intra frame.

Instead, we propose to use smaller QPs in LR inter frame, and relatively larger QPs in HR intra frame in connection with subsequent CRS enhancement⁸, i.e.,

$$\text{QP}_{\text{inter}} = \text{QP}_{\text{intra}} - \delta_{\text{QP}}. \quad (14)$$

δ_{QP} is an offset for balancing the R-D trade-off. Currently, we assume the fixed QPs for all LR inter frames to simplify the problem. Thanks to the advanced inter prediction tools in VVC, such setting in Eq (14) does not greatly increase the bits consumption of LR inter frames. But, it could noticeably improve the reconstruction quality, by which the impact of compression noise can be significantly reduced by preserving relatively more high-frequency details.

Referring to (14), we only need to determine the δ_{QP} for QP allocation across HR intra and LR inter frames in a GoP. A straightforward way is enforcing the frame-level R-D optimization to traverse all potential QP pairs in a GoP to decide the best δ_{QP} for globally optimal coding performance. Apparently, this method is too expensive for applications. As motivated by the design of QP settings in hierarchical B frames, we resort to a simple fixed QP offset between HR intra and LR inter frame for a balanced trade-off.

⁸Note that VVC anchors would use the default QP settings across intra and inter frames as defined in the VVC reference model for comparative study.

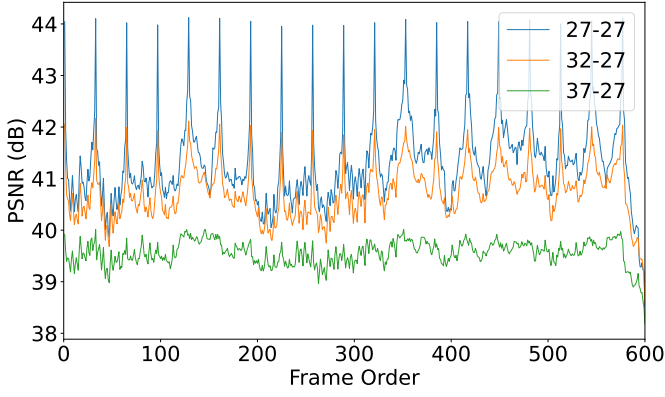


Fig. 6. **Distortion Illustration.** Three QP pairs are conducted for comparison. For instance, “27-27” denotes QP values used for encoding HR intra and LR inter frames respectively in a GoP.

As shown in Fig. 6, we therefore conduct comparisons using three typical QP pairs (e.g., “27-27” for respective HR intra and LR inter frame in a GoP). Given that LR inter frames are encoded using QP 27, when we use QP 37 for encoding HR intra frames, the quality of reference is pretty bad, leading to a much worse reconstruction; If we decreases the QP to 27 for HR intra frame encoding, the quality of restored LR inter frames improves greatly, but the overall bits consumption also increases significantly. Thus, we choose a middle point at QP 32 to compress the HR intra frame. It turns out that the PSNR of reconstructed LR inter frames is close to the case having HR intra frame coded at QP 27 and the bits consumption is much less. By carefully examining other QP pairs and other sequences, we then decide to set $\delta_{QP} = 5$ for well balancing the R-D efficiency.

VI. EXPERIMENTAL STUDIES

This section mainly provides the comparative studies to show the efficiency of proposed CRS-based VVC enhancement. A companion supplemental material is also offered to demonstrate the coding efficiency improvement when plugging proposed CRS module as the enhancement postprocessing for HEVC coder.

A. Implementation Details

1) *Datasets*: We combine the dataset provided in [36] which contains 182 raw videos with various resolutions and contents, and another 15 sequences with resolution of 4K released by [37] for our model training. The first 100 frames of each video are used. Similar to other SR-based video compression enhancement methods, the evaluations of our CRS are mainly conducted under the JVET (Joint Video Exploration Team) Common Test Conditions (CTC) using test sequences with resolution above 720p (e.g., Class A, Class B, Class E) for the RA and LDP configurations. This also fits the practical trend that mainstream imaging devices are now capable of high-definition (HD) and ultra high-definition (UHD) videography. Recent experimental explorations beyond VVC are also focusing on the usage of HD and UHD videos [23].

2) *Video Compression Setup*: For simplicity, our down-sampling operation directly utilizes the bicubic filter offered in FFmpeg⁹, and videos are compressed using the VVC reference software VTM10.0 on a 2.60 GHz Intel Xeon CPU. Targeting for the popular Internet-based video application, this work mainly emphasizes on the scenarios across the intermediate and low bit rate ranges. Thus, the VVC anchor uses CTC QPs, e.g., {32, 37, 42, 47}. In the meantime, the proposed VVC with CRS enhancement applies the QPs with a fixed offset, i.e., {27, 32, 37, 42} for LR inter frames and the same CTC QPs for HR intra frames, with which we can match bit rates for fair comparison. Other SR methods used for comparison follows the similar procedure to select QPs to match the bit rates of VVC anchor. Such comparative study can be easily extended to other QPs or bit rate coverage.

3) *Training Preparation*: In training, three consecutive LR inter frames, their neighboring HR intra frame(s) (two for RA and one for LDP as mentioned in Section IV) and the original uncompressed frame of the target LR inter frame for restoration are randomly cropped into patches with the sizes of 64×64 , 128×128 and 128×128 respectively as grouped training samples. Since our CRS is devised as the decoder-side postprocessing module, both HR intra and LR inter frames are decoded with augmented noises (see (5)). Data augmentation is also done by random flip in horizontal and vertical orientations, and random rotation at 90° , 180° , and 270° . Adam optimizer [38] with default settings is used with learning rate of $1e-4$. We conduct our experiments on PyTorch platform using a Nvidia Titan RTX. We train a model from scratch for each QP value, i.e., total four models are trained in this study.

Previous discussions details the training steps for Y channel only. We use the same procedure to train the model for combined U/V channels by replacing the input and output to match the dimension of U/V planes. As seen the model used for U and V shares the same architecture as that used for Y.

The BD-Rate [24] results are provided to quantitatively evaluate the performance of our CRS and other solutions.

B. Performance Evaluation with VVC Anchor

We first evaluate the compression efficiency of proposed CRS in comparison to the VVC anchor.

1) *Quantitative and Qualitative Gains*: As in Table II and Table III for luminance component, our CRS using default bicubic filter for input sampling, e.g., CRS (bicubic)¹⁰, shows clear performance lead against the VVC anchor, having averaged 8.76% and 11.93% BD-Rate improvements across all test sequences for respective RA and LDP encoder settings. We also exemplify the lanczos filter for input sampling in RA configuration, e.g., CRS (lanczos), having slightly better BD-Rate gain at 9.53% on average.

In the meantime, Figure 7 visualizes the reconstructions of both VVC anchor in RA configuration and our CRS-based VVC enhancement using default bicubic filter to sample

⁹<http://ffmpeg.org/>

¹⁰We also use the “CRS” to represent the case using default bicubic filter for input sampling.

TABLE II

BD-RATE GAINS (%) OF SEVERAL SR METHODS AND OUR PROPOSED CRS AGAINST VVC ANCHOR WITH RA CONFIGURATION. (THE BEST RESULTS ARE HIGHLIGHTED IN BOLD AND THE NUMBER WITH UNDERLINE MEANS NEGATIVE R-D PERFORMANCE, WHICH IS THE SAME BELOW.)

Class	Sequence	bicubic (bicubic)	lanczos (lanczos)	RCAN (bicubic) [15]	EDVR (bicubic) [16]	CRS (bicubic)	CRS (lanczos)
A (4k)	Tango2	-7.05	-2.43	-11.03	-11.65	-12.07	-12.96
	FoodMarket4	-6.26	-0.64	-10.67	-11.03	-11.26	-11.71
	Campfire	-5.18	-4.28	-12.73	-13.87	-16.83	-18.80
	CatRobot	<u>3.78</u>	<u>5.10</u>	-6.62	-7.04	-12.62	-13.14
	DaylightRoad2	<u>6.44</u>	<u>7.43</u>	-5.55	-6.28	-13.86	-14.77
	ParkRunning3	-1.07	-1.21	-6.89	-7.23	-8.54	-8.69
B (1080p)	MarketPlace	<u>2.29</u>	<u>3.24</u>	-4.78	-5.32	-9.57	-10.05
	RitualDance	<u>3.19</u>	<u>4.34</u>	-4.87	-6.05	-9.69	-10.24
	Cactus	<u>46.99</u>	<u>40.96</u>	<u>13.64</u>	<u>8.79</u>	-6.41	-7.29
	BasketballDrive	<u>75.20</u>	<u>66.35</u>	<u>22.13</u>	<u>17.82</u>	<u>1.58</u>	0.05
	BQTerrace	<u>210.48</u>	<u>164.53</u>	<u>59.61</u>	<u>53.04</u>	-0.06	-1.22
	FourPeople	<u>75.06</u>	<u>62.43</u>	<u>21.18</u>	<u>14.92</u>	-12.80	-12.88
E (720p)	Johnny	<u>75.61</u>	<u>67.63</u>	<u>25.99</u>	<u>21.03</u>	-1.20	-2.48
	KristenAndSara	<u>165.85</u>	<u>135.46</u>	<u>39.05</u>	<u>32.67</u>	-9.76	-9.27
Class A		-1.56	0.66	-8.92	-9.52	-12.53	-13.35
Class B		<u>67.63</u>	<u>55.88</u>	<u>17.15</u>	<u>13.66</u>	-4.83	-5.75
Class E		<u>105.51</u>	<u>88.51</u>	<u>28.74</u>	<u>22.87</u>	-7.92	-8.21
Overall		<u>46.10</u>	<u>39.21</u>	<u>8.46</u>	<u>5.7</u>	-8.76	-9.53

TABLE III

BD-RATE GAINS (%) OF SEVERAL SR METHODS AND OUR PROPOSED CRS AGAINST VVC ANCHOR WITH LDP CONFIGURATION.

Class	Sequence	bicubic (bicubic)	RCAN (bicubic) [15]	EDVR (bicubic) [16]	CRS (bicubic)
A (4k)	Tango2	-6.64	-9.15	-17.14	-14.26
	FoodMarket4	-9.52	-11.51	-14.27	-14.47
	Campfire	-10.98	-17.55	-19.25	-25.55
	CatRobot	<u>4.40</u>	-1.77	-10.16	-21.61
	DaylightRoad2	<u>4.34</u>	-3.41	-7.48	-11.51
	ParkRunning3	-8.28	-12.47	-18.82	-18.24
B (1080p)	MarketPlace	1.65	-4.14	-8.86	-8.33
	RitualDance	-0.17	-6.08	-11.63	-9.83
	Cactus	<u>38.79</u>	<u>14.34</u>	<u>6.44</u>	-15.65
	BasketballDrive	<u>54.40</u>	<u>14.56</u>	<u>4.95</u>	2.52
	BQTerrace	<u>143.68</u>	<u>55.63</u>	<u>54.86</u>	35.53
	FourPeople	<u>56.69</u>	<u>19.31</u>	<u>20.72</u>	-27.05
E (720p)	Johnny	<u>47.07</u>	<u>17.61</u>	<u>10.67</u>	-13.51
	KristenAndSara	<u>91.15</u>	<u>31.00</u>	<u>26.84</u>	-25.07
Class A		-4.45	-9.31	-14.52	-17.61
Class B		<u>47.67</u>	<u>14.86</u>	<u>9.15</u>	0.85
Class E		<u>64.97</u>	<u>22.64</u>	<u>19.41</u>	-21.88
Overall		<u>29.04</u>	<u>6.17</u>	<u>1.21</u>	-11.93

the input video. For a fair comparison, the selected frames have almost the same PSNR with partial regions zoomed in for details. Our CRS scheme even offers slightly better texture details at a noticeable bit rate saving. For example, we have observed $\approx 20\%$ bit rate reduction for sequence “DaylightRoad2”, and $\approx 12\%$ reduction for sequence “Tango”.

2) *Complexity*: The encoding time of our proposed method and the VVC anchor is depicted in Fig. 8 for Class A, B, and E in RA configuration. It shows that average 32.2% encoding time reduction is obtained by our proposed method. This is mainly because all the inter frames in our method are encoded at a lower resolution. Note that the reduction percentage differs for various resolutions and QPs. For Class E sequences, due to their relatively stationary scenes, VVC encoding mode can be quickly determined by analysing block distance or motion intensity, thus reducing the encoding time.

Our proposed CRS and other SR methods are applied as the postprocessing module to VVC decoding. Thus, additional

computational complexity is required. Model parameters and GPU running time (in seconds) for class E are shown in Table IV in comparison to other SR methods. Our proposed algorithm requires much less parameters, but the running time is slightly more than EDVR due to non-local affinity computation in TCN. Currently, we enforce the exhaustive computation of affinity map by searching all patches, which is more or less like the full-frame motion search in video codec and hence increases the time cost.

We also report the end-to-end running time of encoder and decoder for our method compared with the VVC anchor. Taking class E coded at QP 32 as an example, since the frame decoding is extremely fast (e.g., milliseconds) and negligible, we use the encoding time as the total running time for VVC anchor. Since the decoder-side CRS takes extra time for reconstruction thus the total running time includes the time used for encoding HR intra and LR inter frames and the model inference time for final reconstruction. As a result, the total



Fig. 7. **Qualitative Visualization.** VVC anchor in RA configuration (top) and proposed CRS-based method (bottom) for each snapshot. The respective bit rate (in kbps) and PSNR (in dB) from top to bottom are: Tango2 (VVC: 1044.50/35.61, CRS: 916.55/35.66), DaylightRoad2 (VVC: 1139.81/33.35, CRS: 918.25/33.45). **Zoom in for more details.**

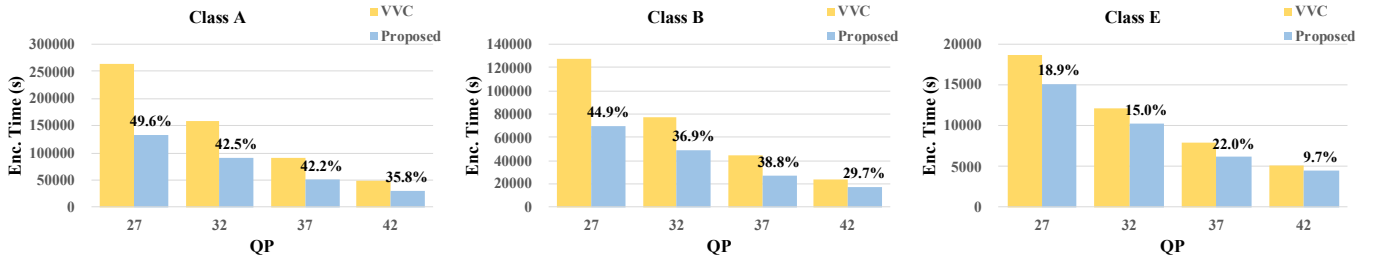


Fig. 8. **Complexity Reduction.** Encoding time of our proposed method compared with the VVC anchor for Class A, B, and E across different QPs. The encoding time reduction percentages are annotated on the top of each bar for the proposed method.

running time of VVC anchor is about 18,666 seconds while our method is 16,466 seconds. Clearly our method still has about 11.79% reduction over VVC.

C. Performance Comparison to Other SR-Based VCE

As aforementioned, built upon the advancements of deep learning techniques, super-resolution (SR) techniques have been greatly improved for information restoration, which can be then utilized as the decoder-side enhancement for promoting overall compression efficiency. Different from our proposed CRS approach, existing SR-based VCE typically samples resolution uniformly and then fully relies on SR algo-

rithms to characterize compression and resampling variations for loss restoration.

We report the efficiency of SR-based VVC enhancement using two typical examples. The first example is re-training popular state-of-the-art SR algorithms, e.g., single-image SR based RCAN [15] and video SR method - EDVR [16] for VVC enhancement. Both RCAN and EDVR are re-trained using the same dataset as ours for fair comparison. In the meantime, bicubic-based upsampling at decoder is provided to match the default bicubic downsampling as the benchmark. Since another lanczos filter outperforms default bicubic method, we also examine the performance of the lanczos filter solely, or together with the CRS in RA profile (e.g., lanczos (lanczos)

TABLE IV
COMPLEXITY COMPARISON OF CRS AND OTHER SR METHODS FOR VVC
ENHANCEMENT. RUNNING TIME HERE IS ONLY PRESENTED FOR
SUPER-RESOLVING A DECODED FRAME ON AVERAGE.

Method	param. (M)	running time (s)
RCAN [15]	12.53	0.48
EDVR [16]	19.67	0.94
CRS	4.25	1.16

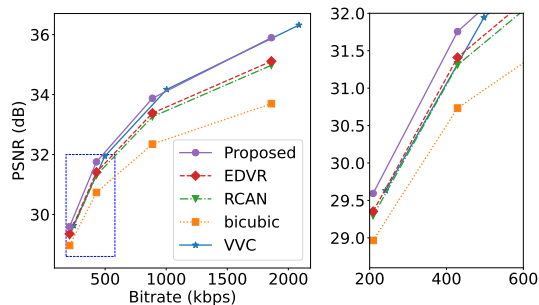


Fig. 9. **R-D Plots.** Averaged compression efficiency of SR-based VVC enhancement against the VVC anchor is presented for Class B sequences in RA configuration. The bitrate from 200 kbps to 600 kbps are zoomed in for a better presentation.

and CRS (lanczos) in Table II).

In addition, we present the JVET EE report on the use of SR algorithms for improving VVC performance, a.k.a., JVET-V0073 [11] and JVET-V0096 [12]. These results include both luminance and chrominance components and are cross-checked by another independent third party.

1) *Retrained SR Models:* As shown in Tables II and III, both RCAN-based and EDVR-based VVC enhancement methods, a.k.a., “RCAN” and “EDVR” for convenience, mainly show positive BD-Rate gains for Class A sequences at 4K resolution, and have very limited improvement for individual sequences in Class B and E at respective 1080p and 720p resolutions. Yet, both RCAN and EDVR based methods produce BD-Rate loss averaged for Class B and E, and for all Classes. On the contrary, our CRS-based VVC enhancement presents positive BD-Rate gains on most sequences across Class A, B and E, with the exceptions of “BasketballDrive” in RA case, and both “BasketballDrive” and “BQTerrace” in LDP case. The loss may come from the large camera motion presented in these two sequences, while default GoP settings used in CTC configuration fix the placement of intra frames which can not well match the camera movement for accurate scenecut. It then leads to possible occlusions that objects in LR inter frames are not previously presented in HR intra frame, which would degrade the quality of super-resolved LR inter frames without appropriate high-frequency components learned from corresponding HR intra frame in the same GoP.

Even for 4K resolution, bicubic upsampling-based SR approach presents inferior coding efficiency to the VVC anchor at some sequences, e.g., “CatRobot” and “DaylightRoad2” for both RA and LDP cases. On average, learning-based SR methods, e.g., RCAN [15] and EDVR [16], greatly improve the enhancement performance from the bicubic upsampling. As for RA setting in Table II, BD-Rate loss is reduced from

46.10% of bicubic upsampling-based solution to the 5.7% of EDVR-based approach. This is because both RCAN [15] and EDVR [16] leverage powerful DNNs to characterize the content variations induced by the resolution resampling and compression.

Occasionally, we notice that the EDVR-based VVC enhancement provides slightly better R-D efficiency than our CRS-based solution for several sequences encoded using LDP configuration, e.g., “Tango2” and “ParkRunning3” in Class A, and “MarketPlace” and “RitualDance” in Class B. It is mainly because only the first frame in a GoP is considered as the HR intra frame following the CTC, and the performance of TCN may be limited in restoring LR inter frames that are far away from the first HR intra picture. Besides, EDVR applies more neighbour frames (4 frames) than ours (two closest neighbor frames) to help the super resolution.

Surprisingly, bicubic upsampling, RCAN and EDVR present all negative efficiency for Class E sequences in both RA and LDP scenarios, while our CRS approach offers clear gains instead. These sequences are video conferencing content, having relatively stationary activities with small temporal motion. Having the HR intra frame as the reference can well compensate the high-frequency components loss incurred in succeeding LR inter frames, which is much better than only exploring spatial correlations with current frame in bicubic or RCAN, and even augmenting temporal correlations across multiple low-resolution frames from the past in EDVR (i.e., high frequency components are still missing in LR frames).

We further plot R-D curves averaged for all Class B sequences with RA configuration in Fig. 9. We can see clearly that only our method shows consistent gains across a wide bit rate range while existing SR methods only present superior performance for a very limited bit rate range, as compared with the VVC anchor. Note that the performance lead of our method against others gets less at critical low bit rates, because in these scenarios, compression noise severely degrades the capability of all algorithms. However, the lead become larger when bit rate increases. It is because the improved quality of HR intra frame can offer a great amount of help for the reconstruction of subsequent LR inter frames.

2) *JVET EE Summary:* In this comparative study, another two SR-based VVC enhancement methods, e.g., JVET-V0073 [11] and JVET-V0096 [12] are used. Both JVET-V0073 [11] and JVET-V0096 [12] apply the Reference Picture Resampling (RPR) adopted in VVC to uniformly sample all frames of input video to a lower spatial resolution, and utilize the VVC to compress downscaled video. Decoded frames will be upscaled using single frame SR methods for restoration. In JVET-V0073 [11], it uses a lightweight network model which is simplified from [39] and consists of 12 convolutional layers, and in the meantime, it updates model parameters with additional bit rate consumption for different content and different QPs; On the contrary, for JVET-V0096 [12], it fully relies on a deeper network modified from [30] to characterize the spatial texture pattern for information restoration.

We present the performance of Class A sequences in both luminance (Y) channel and chrominance (U/V) channels. It should be noted that the models for U and V channels are

TABLE V
BD-RATE GAINS (%) OF JVET-V0073 [11], JVET-V0096 [12] AND OUR CRS-BASED VVC ENHANCEMENTS AGAINST VVC ANCHOR WITH RA CONFIGURATION FOR ALL LUMINANCE (Y) AND CHROMINANCE (UV) CHANNELS.

Sequence	JVET-V0073 [11]			JVET-V0096 [12]			CRS		
	Y	U	V	Y	U	V	Y	U	V
Tango2	-9.78	-7.64	-0.21	-8.55	-11.38	1.09	-11.04	-1.84	-3.72
FoodMarket4	-10.77	2.04	0.55	-7.54	2.47	2.17	-8.67	-6.52	-2.85
Campfire	-15.34	13.61	3.29	-17.42	62.18	-0.25	-16.89	-1.09	-21.51
CatRobot	-4.63	18.22	23.62	2.51	16.39	29.59	-9.49	-10.16	-8.96
DaylightRoad2	-0.57	-0.03	1.09	12.90	-1.02	12.75	-10.99	-17.39	-23.39
ParkRunning3	-11.17	114.24	51.05	-9.44	152.02	64.41	-7.50	43.51	10.17
Overall	-8.71	23.41	13.23	-4.59	36.78	18.29	-10.76	1.09	-8.38

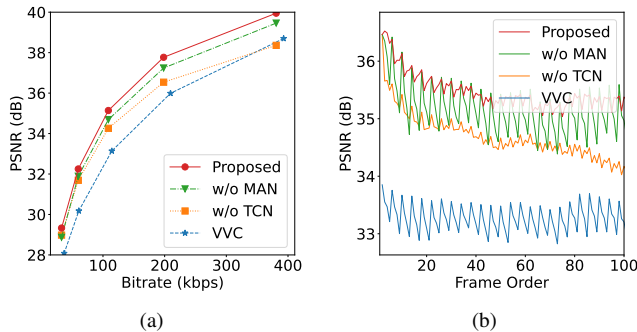


Fig. 10. **Modular Contribution.** Coding efficiency impacts of different modules in CRS evaluated on class E with LDP configuration for a clear presentation. (a) averaged rate-distortion plots; (b) frame-wise snapshots; other sequences have the similar behavior.

trained using the same architecture and procedure as the Y channel. As shown in Table V, the proposed CRS still presents clear performance lead to others when compared with the VVC anchor. Though both JVET-V0073 [11] and JVET-V0096 [12] show about -8.7% and -4.6% BD-Rate improvement for Y components, they have tremendous loss on U/V channels, especially for U channel, e.g., more than 23% and 36% BD-Rate loss respectively. Except for the U channel, our CRS provides positive gains on both Y and V components on average. The loss of coding efficiency on U/V components of proposed CRS mainly comes from a single sequence “ParkRunning3”, while the losses of JVET-V0073 [11] and JVET-V0096 [12] are extremely large, e.g., about 114% and 153% BD-Rate increase. Possible reasons could be the inferior representation of grassland and tree leaves in this video, which is worth for further investigation in our future work.

D. Ablation Study

To fully understand the capabilities of our CRS, we dissect it and examine its modular components.

1) *Modular Contribution.*: In Fig. 10(a), the option “w/o TCN” just turns off the TCN, “w/o MAN” only removes the MCN, and the “Proposed” is the native CRS with all options enabled. In addition, we also offer the VVC anchor for better comparative illustration.

The TCN offers more than 0.7 dB gains on average particularly at high bit rates; The MAN provides nearly 0.4 dB gain on average. This reveals the efficiency of TCN by

compensating LR inter frames with critical high-frequency components from HR intra frame.

Frame-wise gains are consistently presented by the “TCN”, and “MAN” in a GoP snapshot shown in Fig. 10(b). Our proposed CRS with all options enabled achieves consistent advantage across the entire GoP frames and shows less inter frame quality fluctuation due to the use of temporal neighbors in a sliding window, which generate more smooth reconstructed results.

Note that several intermediate frames may have better PSNR by disabling the MAN, e.g., green peaks in Fig. 10(b). We suspect that the deformable alignment may incur the negative effect because of the temporal instability. Whereas, the overall performance is more stable when having MAN enabled.

Furthermore, we have also noticed that error propagation across inter frames makes the quality drop much faster than the native VVC in Fig. 10(b). This may be incurred by noises (e.g., re-sampling, quantization) aggregation across predictive frames, which is worth for further study.

2) *Codec Agnostic.*: Our CRS and other SR methods are used for video compression enhancement as a postprocessing module. Even though this work mainly investigates the VVC enhancement, we expect the method can be extended to other video coding standards as well.

Therefore, we have conducted evaluations when having the HEVC reference model HM16.0 (<https://hevc.hhi.fraunhofer.de>) as the compression engine and test anchor. As reported in the supplemental material along this paper, we show that our method consistently outperforms the standard HEVC model with almost 1 dB gain (or equivalent $\approx 20\%$ BD-Rate improvement). In addition, another popular codec AV1 (<https://aomedia.org/>) is also included for evaluation with about 18% BD-Rate reduction with commonly used LDP profile. More details can be found at <https://njuvision.github.io/CRS/>. Another interesting observation is that by comparing the gains across the HEVC, AV1, and VVC, the coding improvements from the proposed CRS reduce gradually, with about 20% for HEVC, 18% for AV1 and only about 12% for VVC. It reveals that as the compression efficiency of inter coding improves, the potential benefit of applying our CRS declines.

VII. CONCLUSION

The proposed CRS offers an alternative and promising solution for future video coding beyond VVC. Our CRS is a postprocessing module at decoder side, which can be

implemented with almost all popular video codecs, currently reporting remarkable R-D improvements against the VVC anchor and other state-of-the-art methods. The superior efficiency of proposed CRS mainly comes from the effective usage of spatiotemporal correlations, e.g., temporal motion smoothness and spatial texture details, at different resolution granularity for low-resolution frame super-resolution.

There are a variety of interesting topics for future study. For instance, adaptive re-sampling of inter frame is expected to further improve the coding efficiency. In the meantime, targeting for the industrial standard, algorithm complexity is another critical factor for investigation. Furthermore, integrating the CRS enhancement into the coding loop for block-based optimization is also worth for deep exploration.

ACKNOWLEDGEMENT

We are greatly indebted to anonymous reviewers for their valuable comments, and we are very grateful for JVET experts involved in relevant exploration experiments to cross check our approach and discuss with us for further improvements [23].

REFERENCES

- [1] T. Wiegand, G. J. Sullivan, G. Bjøntegaard, and A. Luthra, "Overview of the h.264/avc video coding standard," *IEEE Transactions on Circuits and Systems for Video Technology*, vol. 13, no. 7, pp. 560–576, 2003. 1
- [2] G. J. Sullivan, J. Ohm, W. Han, and T. Wiegand, "Overview of the high efficiency video coding (hevc) standard," *IEEE Transactions on Circuits and Systems for Video Technology*, vol. 22, no. 12, pp. 1649–1668, 2012. 1
- [3] T. Chen, H. Liu, Q. Shen, T. Yue, X. Cao, and Z. Ma, "Deepcoder: A deep neural network based video compression," in *2017 IEEE Visual Communications and Image Processing (VCIP)*. IEEE, 2017, pp. 1–4. 1
- [4] G. Lu, W. Ouyang, D. Xu, X. Zhang, C. Cai, and Z. Gao, "Dvc: An end-to-end deep video compression framework," in *Proceedings of the IEEE Conference on Computer Vision and Pattern Recognition*, 2019, pp. 11 006–11 015. 1
- [5] O. Rippel, S. Nair, C. Lew, S. Branson, A. G. Anderson, and L. Bourdev, "Learned video compression," in *Proceedings of the IEEE International Conference on Computer Vision*, 2019, pp. 3454–3463. 1
- [6] H. Liu, M. Lu, Z. Ma, F. Wang, Z. Xie, X. Cao, and Y. Wang, "Neural video coding using multiscale motion compensation and spatiotemporal context model," *accepted by IEEE Trans. Circuits and Systems for Video Technology*, 2020. 1, 5
- [7] R. Yang, M. Xu, Z. Wang, and T. Li, "Multi-frame quality enhancement for compressed video," in *Proceedings of the IEEE Conference on Computer Vision and Pattern Recognition (CVPR)*, June 2018. 1, 4
- [8] M. Lu, M. Cheng, Y. Xu, S. Pu, Q. Shen, and Z. Ma, "Learned quality enhancement via multi-frame priors for hevc compliant low-delay applications," in *2019 IEEE International Conference on Image Processing (ICIP)*, 2019, pp. 934–938. 1
- [9] J. Tong, X. Wu, D. Ding, Z. Zhu, and Z. Liu, "Learning-based multi-frame video quality enhancement," in *2019 IEEE International Conference on Image Processing (ICIP)*, 2019, pp. 929–933. 1
- [10] Z. Guan, Q. Xing, M. Xu, R. Yang, T. Liu, and Z. Wang, "Mfqc 2.0: A new approach for multi-frame quality enhancement on compressed video," *IEEE Transactions on Pattern Analysis and Machine Intelligence*, vol. 43, no. 3, pp. 949–963, 2021. 1
- [11] T. Chujoh and T. Ikai, "EE1.2: additional experimental results of nn-based super resolution," *JVET Doc. V0073*, April 2021. 1, 2, 11, 12
- [12] A. Kotra, K. Reuze, J. Chen, H. Wang, M. Karczewicz, and J. Li, "EE1-2.3: neural network-based super resolution," *JVET Doc. V0096*, April 2021. 1, 2, 11, 12
- [13] H. Chen, M. Lu, Z. Ma, X. Zhang, Y. Xu, Q. Shen, and W. Zhang, "Learned resolution scaling powered gaming-as-a-service at scale," *IEEE Transactions on Multimedia*, 2020. 1
- [14] W. T. Freeman, T. R. Jones, and E. C. Pasztor, "Example-based super-resolution," *IEEE Computer Graphics and Applications*, vol. 22, no. 2, pp. 56–65, 2002. 1
- [15] Y. Zhang, K. Li, K. Li, L. Wang, B. Zhong, and Y. Fu, "Image super-resolution using very deep residual channel attention networks," in *Proceedings of the European Conference on Computer Vision (ECCV)*, September 2018. 1, 2, 3, 9, 10, 11
- [16] X. Wang, K. C. Chan, K. Yu, C. Dong, and C. Change Loy, "Edvr: Video restoration with enhanced deformable convolutional networks," in *Proceedings of the IEEE/CVF Conference on Computer Vision and Pattern Recognition (CVPR) Workshops*, June 2019. 1, 2, 3, 4, 5, 9, 10, 11
- [17] M. Shen, P. Xue, and C. Wang, "Down-sampling based video coding using super-resolution technique," *IEEE Transactions on Circuits and Systems for Video Technology*, vol. 21, no. 6, pp. 755–765, 2011. 1, 3
- [18] F. Brandi, R. de Queiroz, and D. Mukherjee, "Super resolution of video using key frames," in *2008 IEEE International Symposium on Circuits and Systems*, 2008, pp. 1608–1611. 1
- [19] K. Fischer, C. Herglotz, and A. Kaup, "On versatile video coding at uhd with machine-learning-based super-resolution," in *2020 Twelfth International Conference on Quality of Multimedia Experience (QoMEX)*, 2020, pp. 1–6. 1, 3
- [20] X. Zhu, H. Hu, S. Lin, and J. Dai, "Deformable convnets v2: More deformable, better results," in *Proceedings of the IEEE/CVF Conference on Computer Vision and Pattern Recognition (CVPR)*, June 2019. 2, 3, 5
- [21] Z. Zhang, Z. Wang, Z. Lin, and H. Qi, "Image super-resolution by neural texture transfer," in *Proceedings of the IEEE/CVF Conference on Computer Vision and Pattern Recognition (CVPR)*, June 2019. 2, 6
- [22] F. Yang, H. Yang, J. Fu, H. Lu, and B. Guo, "Learning texture transformer network for image super-resolution," in *Proceedings of the IEEE/CVF Conference on Computer Vision and Pattern Recognition (CVPR)*, June 2020. 2, 6
- [23] E. Alshina, S. Liu, W. Chen, Y. Li, R.-L. Liao, Z. Ma, and H. Wang, "EE1: summary of exploration experiments on neural network-based video coding," *JVET Doc. V0023*, April 2021. 2, 4, 8, 13
- [24] G. Bjøntegaard, "Calculation of average psnr differences between rd-curves," *VCEG-M33*, 2001. 2, 8
- [25] R. Rassool, "Vmaf reproducibility: Validating a perceptual practical video quality metric," in *2017 IEEE International Symposium on Broadband Multimedia Systems and Broadcasting (BMSB)*, 2017, pp. 1–2. 2
- [26] D. Barreto, L. D. Alvarez, R. Molina, A. K. Katsaggelos, and G. M. Callicó, "Region-based super-resolution for compression," *Multidimensional Syst. Signal Process.*, vol. 18, no. 2–3, p. 59–81, Sep. 2007. 3
- [27] F. Brandi, R. de Queiroz, and D. Mukherjee, "Super-resolution of video using key frames and motion estimation," in *2008 15th IEEE International Conference on Image Processing*, 2008, pp. 321–324. 3
- [28] M.-M. Ho, G. He, Z. Wang, and J. Zhou, "Down-sampling based video coding with degradation-aware restoration-reconstruction deep neural network," in *MultiMedia Modeling*. Cham: Springer International Publishing, 2020, pp. 99–110. 3
- [29] K. He, X. Zhang, S. Ren, and J. Sun, "Deep residual learning for image recognition," in *Proceedings of the IEEE Conference on Computer Vision and Pattern Recognition (CVPR)*, June 2016. 3, 4, 7
- [30] B. Lim, S. Son, H. Kim, S. Nah, and K. Mu Lee, "Enhanced deep residual networks for single image super-resolution," in *Proceedings of the IEEE Conference on Computer Vision and Pattern Recognition (CVPR) Workshops*, July 2017. 3, 11
- [31] W. Shi, J. Caballero, F. Huszar, J. Totz, A. P. Aitken, R. Bishop, D. Rueckert, and Z. Wang, "Real-time single image and video super-resolution using an efficient sub-pixel convolutional neural network," in *Proceedings of the IEEE Conference on Computer Vision and Pattern Recognition (CVPR)*, June 2016. 3
- [32] J. Deng, L. Wang, S. Pu, and C. Zhuo, "Spatio-temporal deformable convolution for compressed video quality enhancement," in *Proceedings of the AAAI Conference on Artificial Intelligence*, vol. 34, no. 07, 2020, pp. 10 696–10 703. 5
- [33] S. Woo, J. Park, J.-Y. Lee, and I. S. Kweon, "Cbam: Convolutional block attention module," in *Proceedings of the European Conference on Computer Vision (ECCV)*, September 2018. 5
- [34] M. Cheng, Z. Ma, S. Asif, Y. Xu, H. Liu, W. Bao, and J. Sun, "A dual camera system for high spatiotemporal resolution video acquisition," *IEEE Trans. Pattern Analysis and Machine Intelligence*, 2020. 6
- [35] B. Bross, J. Chen, J.-R. Ohm, G. J. Sullivan, and Y.-K. Wang, "Developments in international video coding standardization after avc, with an overview of versatile video coding (vvc)," *Proceedings of the IEEE*, pp. 1–31, 2021. 7
- [36] T. Li, M. Xu, C. Zhu, R. Yang, Z. Wang, and Z. Guan, "A deep learning approach for multi-frame in-loop filter of hevc," *IEEE Transactions on Image Processing*, vol. 28, no. 11, pp. 5663–5678, 2019. 8

- [37] L. Song, X. Tang, W. Zhang, X. Yang, and P. Xia, "The sjtu 4k video sequence dataset," 07 2013, pp. 34–35. 8
- [38] D. P. Kingma and J. Ba, "Adam: A method for stochastic optimization," 2014. 8
- [39] X. Wang, K. Yu, S. Wu, J. Gu, Y. Liu, C. Dong, Y. Qiao, and C. Change Loy, "Esrgan: Enhanced super-resolution generative adversarial networks," in *Proceedings of the European Conference on Computer Vision (ECCV) Workshops*, 2018, pp. 0–0. 11

Supplemental Material

Ming Lu, Tong Chen, Zhenyu Dai, Dong Wang, Dandan Ding, and Zhan Ma, *Senior Member, IEEE*

Abstract—This is the companion material for the “Decoder-side Cross Resolution Synthesis for Video Compression Enhancement”, by including the coding efficiency evaluations against the HEVC standard.

Index Terms—Video Coding, Cross Resolution Synthesis, Super Resolution, Deep Learning.

I. HEVC ANCHOR

A. Datasets and Implementation Details

We use the same dataset as in the main body of this submission for model training. The first 100 frames of each video are used. Re-sampling operation directly utilizes the bicubic filter offered in FFmpeg¹, and videos are compressed using HEVC reference software HM16.0² with LDP configuration on a 2.60 GHz Intel Xeon CPU for Internet-based ultra-low-latency video application (e.g., ever-increasing video conferencing).

Test evaluations are conducted using the test sequences (Class B, C, D, and E) of JCT-VC [1]. The HEVC anchors use QPs from {32, 37, 42, 47, 51}, while the CRS applies the QPs with matched bit rates for fair comparison. Such comparative study can be easily extended to other QPs or bitrate coverage. The intra interval or GoP size is set to 1 second. Other GoPs are examined in subsequent ablation studies.

The training details, including the data augmentation, loss function, and evaluation metric, are kept the same as what we have applied for VVC reference.

B. Quantitative Comparison

We first evaluate the compression efficiency of proposed CRS in comparison to the HEVC anchor using reference model HM (a.k.a., HEVC anchor for short). As shown in Table I, our method consistently outperforms the standard HEVC with almost 1 dB gain (or equivalent $\approx 25\%$ BD-rate improvement). More than 1.5 dB gain can be observed for fast-motion “BasketballDrive” at 50 FPS (Frame Per Second) and slow-motion “vidyo1” at 60 FPS. Additionally, up to 1.12 dB improvements is also obtained for “Kimono” at 24 FPS. All of these have reported the generalization of CRS to videos with various content characteristics, e.g., fast/slow-motion, high/low-frame rate, rich textures, etc.

We also offer comparative studies to super-resolution-based video coding using the state-of-the-art SISR method - RCAN [2] and video super-resolution method - EDVR [3]. In the meantime, bicubic-based upsampling is also provided as a benchmark. Both RCAN and EDVR are re-trained using

TABLE I
BD-RATE AND BD-PSNR OF PROPOSED CRS AGAINST HEVC ANCHOR
(1-SECOND GOP USED IN LDP COMMON TEST)

Class	Sequence	BD-Rate(%)	BD-PSNR(dB)
B	Kimono	-29.76	1.12
	ParkScene	-23.33	0.69
	Cactus	-29.99	1.11
	BQTerrace	-17.54	0.52
	BasketballDrive	-25.90	0.94
C	RaceHorses	-12.61	0.36
	BQMall	-22.58	0.93
	PartyScene	-23.48	0.73
	BasketballDrill	-37.28	1.63
D	RaceHorses	-19.78	0.71
	BQSquare	-9.02	0.33
	BlowingBubbles	-23.74	0.75
	BasketballPass	-25.45	1.03
E	vidyo1	-31.57	1.70
	vidyo3	-27.41	1.38
	vidyo4	-30.32	1.53
Average		-24.36	0.97

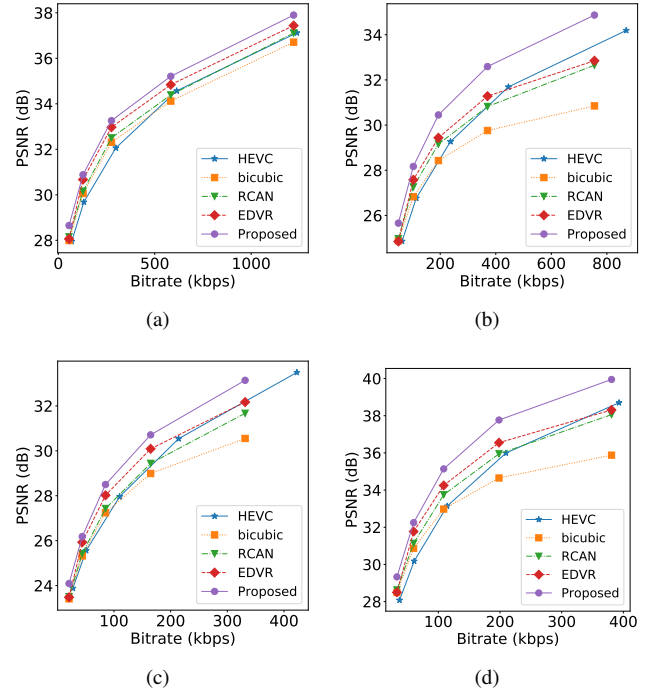


Fig. 1. Rate-distortion curves of proposed CRS, RCAN [2], EDVR [3], bicubic-based video coding, HEVC anchor using reference model - HEVC.

the same dataset for fair comparison. As depicted in Fig. 1, we select one sequence from each class for evaluation. Our CRS shows a clear performance lead against others. Note that the lead is relatively small at critical low bit rates. In these scenarios, compression noise severely degrades the capacity

M. Lu, T. Chen and Z. Ma are with the Nanjing University, Nanjing, China.
Z. Dai and D. Wang are with the OPPO, Inc., Nanjing, China.
D. Ding is with the Hangzhou Normal University, Hangzhou, China.

¹<http://ffmpeg.org/>

²<https://hevc.hhi.fraunhofer.de>

TABLE II
AVERAGED BD-RATE AND BD-PSNR OF PROPOSED CRS AGAINST
HEVC ANCHOR AT VARIOUS GOP SIZE.

GOP	BD-rate(%)	BD-PSNR(dB)
1s	-24.36	0.97
2s	-28.24	1.12
infinity	-20.63	0.83

TABLE III
BD-RATE AND BD-PSNR OF PROPOSED CRS AND HO'S METHOD
AGAINST THE HEVC ANCHOR WITH INFINITY GOP SETTING.

Sequence	BD-Rate (%)		BD-PSNR (dB)	
	Ho [4]	CRS	Ho [4]	CRS
Kimono	-14.5	-30.92	0.50	1.13
ParkScene	-9.99	-27.38	0.24	0.78
Cactus	-2.58	-33.40	0.02	1.23
BasketballDrive	-8.09	-22.47	0.25	0.72

of all algorithms. However, the gains become larger when bit rate increases. It is mainly because the improved quality of STF can offer a great amount of help for the reconstruction of TMFs. Additionally, our CRS shows consistent gains across all bit rates, while existing methods only present the superior performance for a limited bit rate range, over the anchor HEVC.

For the evaluation using VVC codec and VVC anchor in the main body of this submission, we restrict the GoP setting defined in VVC common test condition. For this companion material, we have adjusted the GoP to evaluate its impact on CRS efficiency. This is because most commercial HEVC coders could adaptively set GoP length for better rate-distortion efficiency.

We further examine applications having GoP size at “2 seconds” or “infinity”. For latter case, only the first frame is intra-coded STF, and all the rest frames in a sequence are inter-coded. Table II shows that the coding performance increases from 1-second GoP to the 2-second one, but then drops when having infinity GoP. The loss mainly comes from the scenecuts in a test sequence (e.g., camera moving in BQTerrace). It suggests the optimal coding efficiency of CRS could be possibly achieved when aligning the GoP size with scenecut. Within a scenecut, the first frame can be intra-coded STF and the rest are inter-coded TMFs. Under the same infinity GoP setting, another state-of-the-art super-resolution based video coding algorithm, e.g., Ho’s method [4], which directly down scales all frames before encoding followed by a single image super-resolution at decoder, is also included for comparison using the same HEVC anchor, shown in Table III. Experiments have reported the consistent performance lead ($> 2\times$) of our CRS, even for complex-motion “Cactus”. This further reveals the efficiency by decomposing the video into spatial and temporal attributes for separable processing and final synthesis.

REFERENCES

- [1] J. Ohm, G. J. Sullivan, H. Schwarz, T. K. Tan, and T. Wiegand, “Comparison of the coding efficiency of video coding standards—including

- high efficiency video coding (hevc),” *IEEE Transactions on Circuits and Systems for Video Technology*, vol. 22, no. 12, pp. 1669–1684, 2012. 1
- [2] Y. Zhang, K. Li, K. Li, L. Wang, B. Zhong, and Y. Fu, “Image super-resolution using very deep residual channel attention networks,” in *Proceedings of the European Conference on Computer Vision (ECCV)*, September 2018. 1
- [3] X. Wang, K. C. Chan, K. Yu, C. Dong, and C. Change Loy, “Edvr: Video restoration with enhanced deformable convolutional networks,” in *Proceedings of the IEEE/CVF Conference on Computer Vision and Pattern Recognition (CVPR) Workshops*, June 2019. 1
- [4] M.-M. Ho, G. He, Z. Wang, and J. Zhou, “Down-sampling based video coding with degradation-aware restoration-reconstruction deep neural network,” in *Multimedia Modeling*. Cham: Springer International Publishing, 2020, pp. 99–110. 2